THE ASTROPHYSICAL JOURNAL, 499:221–226, 1998 May 20
© 1998. The American Astronomical Society. All rights reserved. Printed in U.S.A.

SUBPARSEC POLARIMETRIC RADIO OBSERVATIONS OF 3C 120: A CLOSE-UP LOOK AT SUPERLUMINAL MOTION

JOSÉ-LUIS GÓMEZ,[1] ALAN P. MARSCHER,[2] ANTONIO ALBERDI,[1] JOSÉ Mª. MARTÍ,[3] AND JOSÉ Mª. IBÁÑEZ[3]
Received 1997 November 10; accepted 1998 January 5

ABSTRACT

We present two-epoch polarimetric images of the radio galaxy 3C 120 obtained with the Very Long Baseline Array at 22 and 43 GHz. Because of the proximity of 3C 120 ($z = 0.033$), the 43 GHz observations allow us to observe superluminal motions with the highest resolution achieved to date, 0.07 h^{-1} pc. Up to ten different superluminal components, with velocities between 2.3 and 5.4 $h^{-1}c$, can be observed in this active source, with approximately monthly ejections of new components. Polarization is observed in several components and at both frequencies, with peaks in the linearly polarized flux not always coincident with the peaks in total intensity. The orientation of the magnetic field is observed to vary with respect to the jet flow direction as a function of frequency, epoch, and position along the jet.

These observations are in agreement with previous numerical simulations of superluminal sources (Gómez et al. 1997). The classical association of lower frequency components with single shocks does not appear to be valid, and multiple components may be the result of a single disturbance in the jet flow. This is a consequence of the interaction of the shocked plasma with the external medium and the underlying jet, as well as hydrodynamical processes inside the shocked region, neglected in previous analytical shock studies owing to the nonlinearity of the jet fluid dynamics.

Subject headings: galaxies: active — galaxies: individual (3C 120) — galaxies: jets — polarization — radio continuum: galaxies

1. INTRODUCTION

Since the early days of Very Long Baseline Interferometric (VLBI) observations, superluminal motions have been found in the jets of many active galactic nuclei (AGN). This phenomenon can be explained by relativistic fluid motions in jets of magnetized plasma viewed at small angles to the line of sight (Blandford & Königl 1979). The use of models based on ideal hydrodynamics (Blandford & Rees 1974) and a crude approximation of shock waves as square waves (Marscher & Gear 1985; Hughes, Aller, & Aller 1985) successfully interpreted the main characteristics of observed superluminal sources. However, the increasing resolution of VLBI observations, obtained when observing either at millimeter wavelengths or with the inclusion of antennas in orbit, requires more detailed and realistic models. This has become possible through the development of time-dependent hydrodynamical relativistic codes (Duncan & Hughes 1994; Martí, Müller, & Ibáñez 1994) and their implementation in the calculation of the radio emission (Gómez et al. 1995, 1997; Mioduszewski, Hughes, & Duncan 1997; Komissarov & Falle 1997). Following these simulations, Gómez et al. (1997) predicted that the simple superluminal motion observed at lower frequencies would in fact be more complex when observed at higher resolution. The classical association of lower frequency components with single shocks should not be valid, and high-resolution observations should reveal that a single disturbance in the jet flow can cause the appearance of multiple components. Testing these hypotheses requires the highest possible linear resolution. Toward that end, we here present high-frequency VLBI observations of the closest known superluminal source, 3C 120 ($z = 0.033$).

3C 120, usually classified as a Seyfert 1 galaxy, although its optical morphology is also consistent with a broad-line radio galaxy, is a powerful and variable emitter of radiation at all observed frequencies (see Grandi et al. 1997 and references therein). It was one of the first four sources in which superluminal motion was detected on the scale of parsecs (Seielstad et al. 1979; Walker, Benson, & Unwin 1987) to tens of parsecs (Benson et al. 1988; Walker 1997). An optical counterpart of the radio jet has also been detected (Hjorth et al. 1995). These characteristics rank 3C 120 among the most interesting active galaxies.

2. OBSERVATIONS AND DATA ANALYSIS

The observations were performed on 1996 November 11 and December 22, using the NRAO's[4] Very Long Baseline Array (VLBA) at frequencies of 22 and 43 GHz. The data were recorded in 1 bit sampling VLBA format with 32 MHz bandwidth per circular polarization. The reduction of the data was performed within the NRAO Astronomical Image Processing System (AIPS) software in the usual manner (e.g., Leppänen, Zensus, & Diamond 1995). Opacity corrections were introduced by solving for receiver temperature and zenith opacity at each antenna. Fringe fitting in residual delay and fringe rate was performed for both parallel hands independently and referred to a common reference antenna. Delay differences between the right- and left-handed systems were estimated over a short scan of cross-polarized data of a strong calibrator (3C 454.3). The instrumental polarization was determined using the feed solution algorithm developed by Leppänen et al. (1995). The feed D-terms were found to be very consistent between sources and to remain stable during the 41 day interval

[1] Instituto de Astrofísica de Andalucía (CSIC), Apdo. 3004, Granada 18080, Spain; jlgomez@iaa.es, antxon@iaa.es.

[2] Department of Astronomy, Boston University, 725 Commonwealth Avenue, Boston, MA 02215; marscher@bu.edu.

[3] Departamento de Astronomía y Astrofísica, Universidad de Valencia, Burjassot 46100, Spain; Jose-Maria.Marti@uv.es, jose.m.ibanez@uv.es.

[4] The National Radio Astronomy Observatory is a facility of the National Science Foundation operated under cooperative agreement by Associated Universities, Inc.

between the two epochs and at both observing frequencies, with typical values of the order of a few percent. Larger values of 7%–8% were found for the antennas at St. Croix and OVRO at 22 GHz, whereas at 43 GHz such values were found at Hancock, Los Alamos, North Liberty, and Pie Town. Because of snow at Brewster during the second epoch, most of the 43 GHz data from this antenna were deleted.

The absolute phase offset between right and left circular polarizations at the reference antenna was estimated by observing three different calibrators, 3C 454.3, 0420–014, and 0735+178, at both frequencies. Through a comparison with the results reported by Kemball, Diamond, & Paulini-Toth (1996) for 3C 454.3 and 0420–014, and by Gabuzda et al. (1994) for 0735+178 (although at a lower frequency), a common compatible solution for the absolute calibration of the electric vector position angle (EVPA) can be found, but with an error of $\lesssim 30°$. Furthermore, Nartallo et al. (1998) report significant changes in the orientation of the EVPA at millimeter and submillimeter wavelengths in all three sources on timescales of months. 3C 454.3 is also a variable source with frequent ejections of components (Marscher et al. 1998), which makes it difficult to use it as a polarization angle calibrator. However, comparison with other polarimetry observations carried out at similar epochs and the same frequencies revealed a good agreement in the determination of the D-terms (M. Lister & J. Wardle 1997, private communications), and were used to calibrate the EVPA, with an error that we judge to be within 10°.

3. RESULTS

Figures 1 and 2 show the VLBA total and linearly polarized intensity images of 3C 120 at 22 and 43 GHz, respectively. Because of the relative proximity of 3C 120, maps at 43 GHz provide a linear resolution of 0.07 h^{-1} pc ($H_0 = 100\ h$ km s^{-1} Mpc^{-1}), the highest achieved to date for a superluminal source. The images reveal a very complex radio jet in 3C 120. Components have been labeled from west to east, using upper-case letters for the maps at 22 GHz. The separation of only 41 days between the two epochs is enough to reveal multiple components moving at apparently superluminal velocities, a stationary component

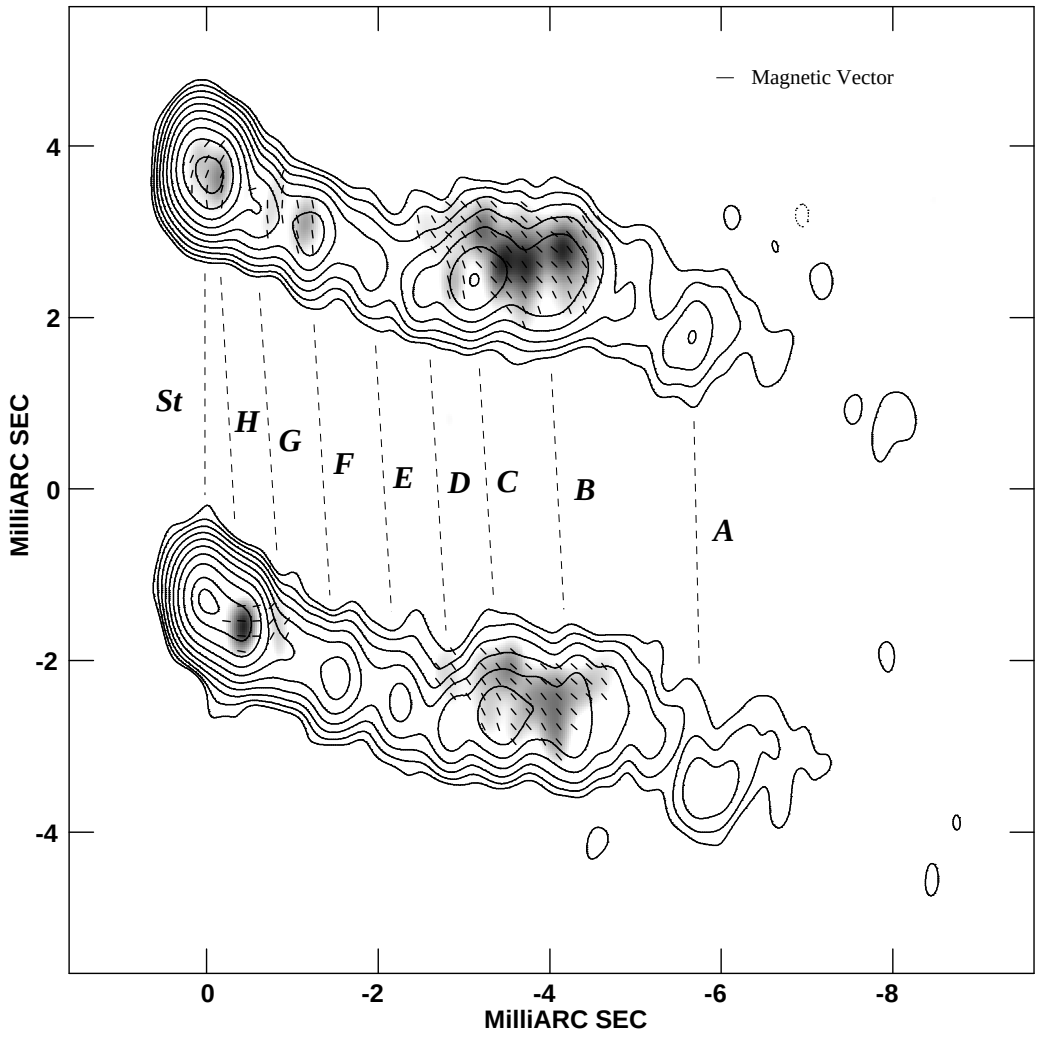

FIG. 1.—VLBI maps of 3C 120 at 22 GHz for epochs 1996 November 11 (*top*) and 1996 December 22 (*bottom*). Total intensity is plotted as contour maps, while the linear gray scale shows the linearly polarized intensity. Lines show the direction of the magnetic field vector. For 1996 November, contour levels are at −0.15%, 0.15%, 0.3%, 0.6%, 1.2%, 2.4%, 4.8%, 9.6%, 19.2%, 38.4%, and 76.8% of the peak at 1.38 Jy beam^{-1}, the convolving beam is 0.63 × 0.29 (FWHM), with position angle −8°, and the maximum in polarized flux is 9.2 mJy, with a noise level of 2 mJy. For 1996 December, contour levels are −0.25%, 0.25%, 0.5%, 1%, 2%, 4%, 8%, 16%, 32%, 64%, and 90% of the peak at 0.86 Jy beam^{-1}, the convolving beam is 0.63 × 0.29, with position angle −5.4°, and the peak in polarized flux is 12.4 mJy, with a noise level of 4.4 mJy.

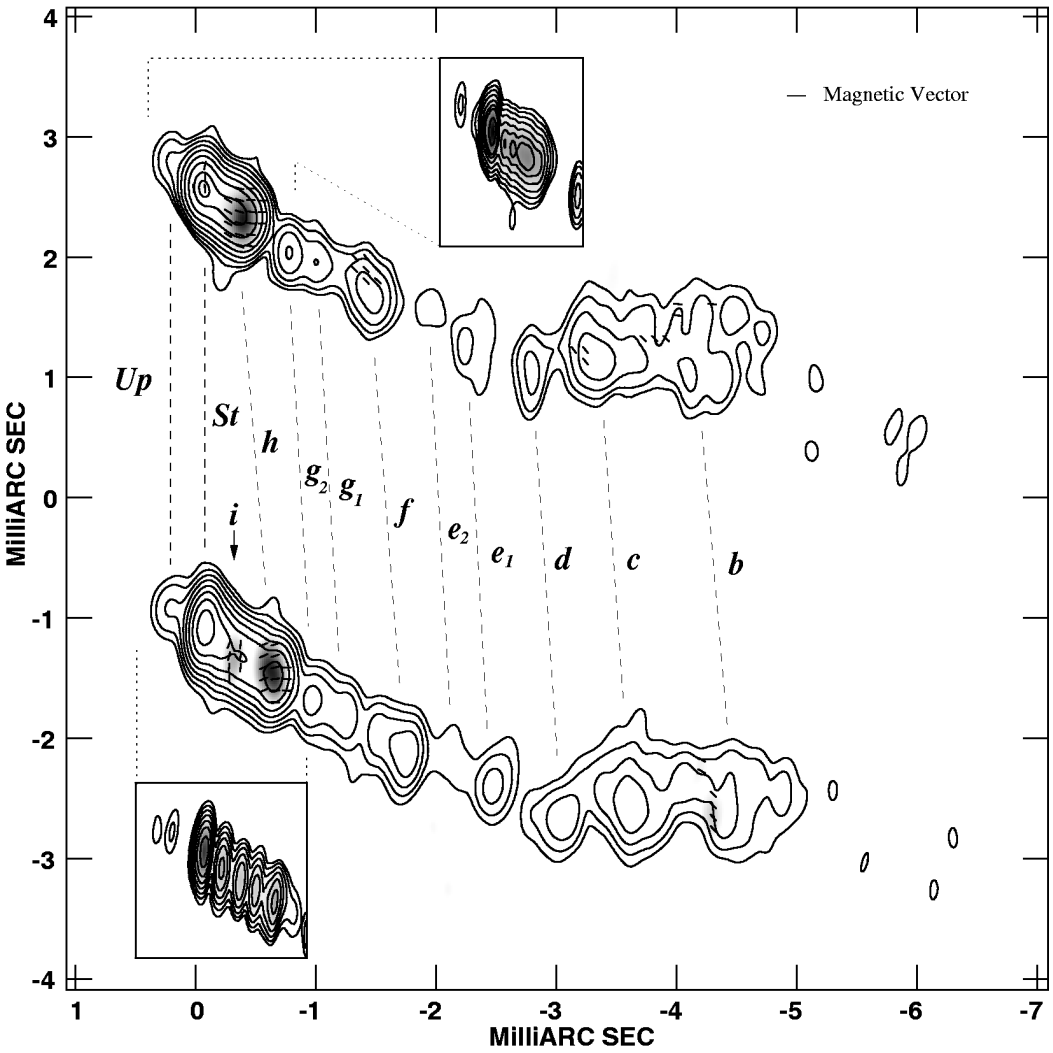

FIG. 2.—Same as Fig. 1, but at 43 GHz. For 1996 November, contour levels are at −0.5%, 0.5%, 1%, 2%, 4%, 8%, 16%, 32%, 64%, and 90% of the peak of 0.82 Jy beam^{-1}, the convolving beam is 0.32 × 0.17 (FWHM), with position angle −2.7°, and the maximum in polarized flux is 39.2 mJy, with a noise level of 2.9 mJy. For 1996 December, contour levels are at −0.5%, 0.5%, 1%, 2%, 4%, 8%, 16%, 32%, and 64% of the peak at 0.63 Jy beam^{-1}, the convolving beam is 0.36 × 0.15, with position angle −6°, and the peak in polarized flux is 10.3 mJy, with a noise level of 2.6 mJy. Insets show, in contours and gray scale, the total intensity emission from the inner region convolved using an overresolved beam of 0.32 × 0.06 mas, with position angles of −3° and −6° for 1996 November and December, respectively.

"St," and an extension of emission east of this component (only resolved at 43 GHz), which we have labeled "Up." Due to the higher resolution achieved at 43 GHz, some of the components observed at 22 GHz split into different components, as occurs for component pairs e_1–e_2 and g_1–g_2. No opacity effects are involved in this splitting, since the spectral index maps for both epochs show an optically thin jet, except for components St and Up, with values $\alpha = 0.2$ and 0.6 (defined such that the flux density $S_\nu \propto \nu^\alpha$), respectively.

Table 1 summarizes the physical parameters obtained for 3C 120 at both frequencies and epochs, as obtained by representing the main features of the images by model components with elliptical Gaussian brightness profiles. The parameters tabulated are the total intensity flux (S), transverse apparent velocity (β), degree of polarization (m), and magnetic field position angle (MFPA) for each component.

3.1. *Proper Motions and Flux Density Evolution*

Different apparent velocities are measured for components A to H (b to h at 43 GHz), with the largest value corresponding to the newly ejected component h. Given the complexities of the images and the difficulty in obtaining reliable error estimations when model-fitting so many components, we regard only component h as having a proper motion significantly different from that of the other components. Using the maximum apparent motion observed in h, we estimate an upper limit to the viewing angle of $\theta = 21°$ ($h = 1$; 14° for $h = 0.65$), and a minimum pattern Lorentz factor of the shock associated with h of $\Gamma_{\rm min} = 5.5$ ($h = 1$; 8.4 for $h = 0.65$). Apparent motions at both frequencies are in general concordance, where the larger discrepancies can be accounted for by considering the changes in the brightness distributions of components, particularly important for H, F, and (combined) B-C, which show significant structure at 43 GHz.

Components A to G show small variation in flux with time, while component H shows at both frequencies a marked decrease in flux of about 0.85 Jy. This, together with its larger proper motion, indicates that component H is traveling under rather different conditions than the rest of components, which suggests a rapid change in the physical

TABLE 1

PHYSICAL PARAMETERS OF 3C 120

COMPONENT		S (mJy)		β_{app} ($h^{-1}c$)		m (%)		MFPA (deg)	
22 GHz	43 GHz	22 GHz	43 GHz	22 GHz	43 GHz	22 GHz	43 GHz	22 GHz	43 GHz
Up	Up.....		19/18		0				
St	St	800/1000	910/866			0.5	0.7	154	13
	i.....		/252				/1		/2
H	h	1588/746	1314/460	3.9	5.5	0.4/1.9	3.4/3.9	158/98	86/114
G	g_2	287/150	72/70	2.9	2.6	2.4/8.4[a]		178/156	
	g_1		45/34		3.8				
F	f.....	211/200	103/89	3.4	4.8	3.2	9.5	2	53
E	e_2	82/100	12/9	3.7	2.8				
	e_1		22/35		3.2				
D	d	136/132	43/55	3.7	3.9				
C[b]	c	365/387	207/167	2.9	4.1	10/12.5	13/8.4	39/48	53/53
B[b]	b	314/312	263/150	2.3	3.2	10/12.5	13/8.4	39/48	53/53
A		43/49		2.9					

NOTE—Second-epoch data are tabulated after a slash. Errors are approximately 5, 0.2, 0.1, and 1 for the total flux, apparent transverse velocity, degree of polarization, and MFPA, respectively. Weaker constraints on the model fitting lead to significantly larger uncertainties for components G, c, and b.

[a] Abnormally high value, most probably due to the large offset between the peaks of the total and polarized fluxes for this component.

[b] Polarization data correspond to mean values for the combined B + C (b + c) region.

properties of the jet and/or ambient medium in this inner region of the jet in 3C 120.

Component St experienced a small increase in flux at 22 GHz between the two observed epochs, and a small decrease at 43 GHz. Component Up, which appears east of St, maintains the same flux density at both epochs, at roughly the same distance from St. Since St is optically thick and (we assume) stationary, this makes St a good candidate for the core of 3C 120, which raises the question of the nature of Up. Unless Up is an artifact of calibration errors, its presence indicates emission upstream the core, which could have two possible explanations. One is that Up corresponds to the counterjet of 3C 120. Indeed, its flux density would be expected to be $\sim[(1 + \beta \cos \theta)/(1 - \beta \cos \theta)]^{2-\alpha}$ times fainter than that of St. Using the values for the flow Lorentz factor and viewing angle of component h given in § 3.1 and $\alpha = 0.6$, the jet:counterjet flux density ratio should therefore be ~ 90 ($h = 1$; 260 for $h = 0.65$), compared to the observed St:Up ratio of ~ 50. Given the large associated uncertainties, this hypothesis cannot be rejected. The second possibility is that Up corresponds to a weak standing shock or some other feature upstream of the site of greatest emission. In this case, the core, St, would represent a strong recollimation shock, as expected theoretically (Daly & Marscher 1988; Gómez et al. 1995, 1997), while Up would be in a region of the jet where the Lorentz factor is lower (as in the accelerating jet model of Marscher 1980) or the electron acceleration not as efficient as at St.

3.2. *Polarization*

Components seen in the images of polarized intensity are not always coincident with maxima in total intensity (see also Kemball et al. 1996). Therefore, we can only obtain estimations of m by the approximation that both maxima are coincident. For the first 22 GHz epoch, most of the polarized flux comes from the B-C region, which has a rather high degree of polarization, $m \sim 10\%$. For this 22 GHz epoch, components F to St are also detected in polarized emission, with m increasing with distance downstream. Between the two epochs, the polarized flux density of component H increases from 6 to 14 mJy, ($m = 0.4$ to 1.9%), with the polarization of components C and B remaining essentially constant.

The images of polarized intensity at 43 GHz show the same positive gradient in m along the jet. The polarized flux at the first epoch is dominated by the recently ejected component h, with a polarized flux of 45 mJy ($m = 3.4\%$). Also marginally detected are components St and f, and components c and b. By the second epoch, component h has decreased its polarized flux to 18 mJy, accompanied by an increase in m to 3.9%. This last epoch also shows emission from a component between St and h, labeled i. The MFPA in i is roughly perpendicular to the jet axis, as is the case for St in the first epoch. This contrasts with component h, which shows an MFPA approximately parallel to the jet axis.

Both frequencies reveal a similar orientation of the magnetic field, except for components F-f and H-h in the first epoch. Component H shows a rotation of 60° in polarization angle at 22 GHz between the two epochs. This rotation is consistent with a change in opacity for component H at 22 GHz (Gómez et al. 1994), due to the blending of H with the optically thick component St at the first epoch. However, this change in opacity cannot account for the frequency-dependent MFPA of component F-f, since it is optically thin at both frequencies.

4. THEORETICAL INTERPRETATIONS AND CONCLUSIONS

Superluminal components A to H in 3C 120 can be interpreted in terms of shock waves traveling relativistically along the jet (see, e.g., numerical simulations by Gómez et al. [1997] and references therein). Since plane-transverse shock waves compress the magnetic field perpendicular to the jet axis, in order to explain the observed MFPAs parallel to the axis by transverse shocks, we need to make the assumption that the field has a large degree of ordering in this direction, with only a small fraction randomly oriented.

A low degree of polarization m is expected, since the compressed magnetic field and components initially parallel to the jet axis will partially cancel. As the component moves downstream, the shock compression decreases, enhancing the perpendicular field less; the net ordering of the magnetic field should therefore increase, resulting in a larger degree of polarization with no rotation of the MFPA. The evolution of the polarization structure of component H-h is well explained within this scheme, together with the opacity effects previously mentioned. The explanation of the 22 GHz polarization structure of components G and F remains uncertain, especially with regard to the discrepancies with the 43 GHz measurements. If a similar nature for components F, G, and H is assumed, the data require a rapid rotation of the magnetic field between the positions of these components or a change in the orientation of the shock fronts with respect to the observer.

The MFPA in the region of components C-B shows a rotation of about 50° with respect to the local direction of the jet flow. As observed previously at larger scales (Walker et al. 1987), these high-frequency maps show a jet that mostly bends gently, but has a sharper change in direction in the region of C-B. The jet trajectory is also consistent with the projection of a very low pitch angle helix, where components C-B would mark a portion of the helix oriented more favorably toward the observer. In this case, numerical simulations of helical jets (Gómez et al. 1994) show a rotation of the magnetic field as observed in 3C 120, with the MFPA indicating the direction of the jet flow in the bend ahead. It is also in this region that the maximum offsets between the polarized and total intensity emission are found. This may also be an indication of the more favorable orientation of the jet with respect to the observer, since a rotation of the plane of compression toward the plane of observation would lead to greater disordering of the projected magnetic field.

The perpendicular orientation to the jet axis of the MFPA in component St can be interpreted under our assumption of a strong oblique (conical) recollimation shock. Numerical simulations (Gómez et al. 1995, 1997) show that such recollimation shocks result in components with high total intensity, and can be used to interpret the cores in compact jets. Cawthorne & Cobb (1990) have shown that such shocks can, under certain values of the viewing angle and other jet parameters, result in an MFPA transverse to the jet flow.

4.1. *The Inner Milliarcsecond of the Jet*

To visualize the inner jet structure of 3C 120, we have included as insets overresolved maps obtained by reducing the size of the minor axis (along the jet flow) of the restoring beam to about half of its proper value. (The splitting of i into three new components, i_1, i_2, and i_3 [not labeled in Fig. 2], is already visible at the second epoch by reducing the size of the beam minor axis by only 20% [not shown].) The inner jet structure then becomes remarkably similar to the computer-generated images presented by Gómez et al. (1997; see their Plate 2), based on relativistic hydrodynamical and emission simulations of shocks in jets. These simulations show that a single shock may appear as multiple components when observed at high linear resolution, and blended as a single component at lower resolution. This is due to the interaction of the shocked fluid with the external medium and the underlying jet, as well as hydrodynamical processes governing the evolution of the plasma inside the shocked region. Although further data would be necessary to constrain a model, we can, in the framework of the results obtained in the numerical simulations, outline three hypotheses:

1. Components i_1, i_2, i_3, and h would correspond to different internal subfeatures of a single shocked region, sr (which at the lower resolution at 22 GHz would appear as the single component H). As can be seen in the simulations of Gómez et al. (1997), these are secondary shocks caused by pressure mismatches at the boundary between the external medium and either the shocked region or the ambient jet. Component h would correspond to the forward shock front of sr. The simulations predict different and variable apparent velocities, as well as fluxes, for the internal features in sr, which under certain circumstances may even show backward motions. Although no upstream motion is observed in the three components of i_1, i_2, and i_3, the first of these (closest to St) shows a subluminal motion of $0.4\ h^{-1}c$, with higher velocities of 2.2 and $2.6\ h^{-1}c$ for the other two—all measured with an estimated error of about $0.3c$. These changes in the brightness distribution of sr (i.e., H) would lead to different apparent motions of the component with time and frequency, thereby explaining the different values obtained at 22 and 43 GHz.
2. Component h corresponds to a single, very thin shock in the jet flow, and components i_1, i_2, and i_3 are associated with internal recollimation shocks, trailing the main shocked region h and generated by surface instabilities caused by interaction of the shocked flow with the external medium.
3. Components i_1, i_2, and i_3, as well as h, are each individual shocks. We find this case to be less plausible, since it would then be more difficult to interpret the proper motions as well as the polarization structure observed in components i_1, i_2, and i_3. It is also doubtful whether a jet can produce shocks so closely spaced, since the simulations show that a disturbance causes both a shock and a trailing rarefaction.

Although further high-frequency VLBI polarimetry observations of 3C 120, in progress, should provide the necessary information to constrain a final model, the current data are in general agreement with the numerical simulations presented in Gómez et al. (1997). This supports the importance of the relativistic hydrodynamical processes that take place in compact jets, and the powerful tool that the simulations represent in the study of parsec-scale jets in AGNs. More detailed numerical modeling (plus enhancement from two-dimensional hydrodynamics to three-dimensional magnetohydrodynamics) of relativistic jets, combined with further high-resolution observations, should lead to a deeper understanding of compact extragalactic jets.

The authors thank M. Lister and J. Wardle for sharing helpful comments as well as data prior to publication, which helped with the MFPA calibration. We are also grateful to the referee, Roberto Fanti, for helpful comments. This research was supported in part by Spain's Direccion General de Investigacion Cientifica y Tecnica (DGICYT) (PB94-1275, PB94-0973) and by NATO grant SA.5-2-05 (CRG.961228). J. L. G. gratefully acknowledges a return grant from the Spanish Ministry of Education and Culture.

REFERENCES

Benson, J. M., Walker, R. C., Unwin, S. C., Muxlow, T. W. B., Wilkinson, P. N., Booth, R. S., Pilbratt, G., & Simon, R. S. 1988, ApJ, 334, 560
Blandford, R. D., & Königl, A. 1979, ApJ, 232, 34
Blandford, R. D., & Rees, M. J. 1974, MNRAS, 169, 395
Cawthorne, T. V., & Cobb, W. K. 1990, ApJ, 350, 536
Daly, R. A., & Marscher, A. P. 1988, ApJ, 334, 539
Duncan, G. C., & Hughes, P. A. 1994, ApJ, 436, L119
Gabuzda, D. C., Wardle, J. F. C., Roberts, D. H., Aller, M. F., & Aller, M. H. 1994, ApJ, 435, 128
Gómez, J. L., Alberdi, A., Marcaide, J. M., Marscher, A. P., & Travis, J. P. 1994, A&A, 292, 33
Gómez, J. L., Martí, J. Mª., Marscher, A. P., Ibáñez, J. Mª., & Alberdi, A. 1997, ApJ, 482, L33
Gómez, J. L., Martí, J. Mª., Marscher, A. P., Ibáñez, J. Mª., & Marcaide, J. M. 1995, ApJ, 449, L19
Grandi, P., Sambruna, R. M., Maraschi, L., Matt, G., Urry, C. M., & Mushotzky, R. F. 1997, ApJ, 487, 636
Hjorth, J., Vestergaard, M., Sørensen, A. N., & Grundahl, F. 1995, ApJ, 452, L17
Hughes, P. A., Aller, H. D., & Aller, M. F. 1985, ApJ, 298, 301
Kemball, A. J., Diamond, P. J., & Pauliny-Toth, I. I. K. 1996, ApJ, 464, L55
Komissarov, S. S., & Falle, S. A. E. G. 1997, MNRAS, 288, 833
Leppänen, K. J., Zensus, J. A., & Diamond, P. J. 1995, AJ, 110, 2479
Marscher, A. P. 1980, ApJ, 235, 386
Marscher, A. P., & Gear, W. K. 1985, ApJ, 298, 114
Marscher, A. P., et al. 1998, in preparation
Martí, J. Mª., Müller, E., & Ibáñez, J. Mª. 1994, A&A, 281, L9
Mioduszewski, A. J., Hughes, P. A., & Duncan, G. C. 1997, ApJ, 476, 649
Nartallo, R., Gear, W. K., Murray, A. G., Robson, E. I., & Hough, J. H. 1998, MNRAS, in press
Seielstad, G. A., Cohen, M. H., Linfield, R. P., Moffet, A. T., Romney, J. D., Schilizzi, R. T., & Shaffer, D. B. 1979, ApJ, 229, 53
Walker, R. C. 1997, ApJ, 488, 675
Walker, R. C., Benson, J. M., & Unwin, S. C. 1987, ApJ, 316, 546